

## Angular-Momentum Effects in Compound-Nucleus Reactions Induced by 27-MeV $^{14}\text{N}$ Ions\*

F. E. DURHAM† AND M. L. HALBERT

*Oak Ridge National Laboratory, Oak Ridge, Tennessee*

(Received 5 October 1964)

The angular distribution of particles emitted in the statistical decay of a compound nucleus will show forward-backward peaking if the angular momentum available in the final system is limited. Furthermore, the decay will not be independent of the mode of formation. These effects were demonstrated by measurements of the energy and angular distributions of alpha particles emitted from reactions of  $^{14}\text{N}$  with  $^{16}\text{O}$ ,  $^{23}\text{Na}$ , and  $^{27}\text{Al}$  at about 27 MeV. The angular distributions were analyzed by the semiclassical theory of Ericson and Strutinski to determine the spin cutoff parameter  $\sigma$ , or equivalently the moment of inertia  $\mathcal{I}$ . The values of  $\sigma$  ranged from 2.6 for the residual nucleus  $^{26}\text{Al}$  to 3.5 for  $^{37}\text{Ar}$ . The moment of inertia was approximately  $0.9 \mathcal{I}_{\text{rigid}}$ . The energy dependence of the level density was determined from the energy spectra. With the simple form  $\exp [2(a_1 E)^{1/2}]$ , good fits were obtained with  $a_1 \approx A/10$  for the two heavier residual nuclei. The data did not distinguish between this expression and the form  $E^{-2} \exp [2(a_2 E)^{1/2}]$ ; equally good fits were obtained with  $a_2 \approx \frac{1}{3}A$ .

### I. INTRODUCTION

IT has long been known<sup>1</sup> that the angular distribution of particles emitted during the statistical decay of a compound nucleus is symmetric about  $90^\circ$ , provided that a suitable average has been made. Isotropy is predicted only if certain further assumptions are made, principally that the dependence of the residual-nucleus level density on the spin  $j$  is proportional to  $(2j+1)$ . For small  $j$  this additional assumption is consistent with existing data. Since not much angular momentum is involved in reactions induced by low-energy protons or neutrons, it is quite common to find nearly isotropic distributions in such reactions after subtraction of the direct-interaction part.

Recently, however, examples of symmetric forward-backward peaking have been found in reactions induced by neutrons,<sup>2-4</sup> alpha particles,<sup>5</sup> and heavier ions.<sup>6,7</sup> Essentially the same effect was discovered earlier in fission of high-spin compound nuclei and explained by Halpern and Strutinski.<sup>8</sup> In a semiclassical approximation Ericson and Strutinski<sup>9</sup> discussed the symmetric forward-backward peaking for reactions involving large angular momentum, and they showed how the distribution of spin states in the final nucleus could be ob-

tained from the angular distribution. A brief statement of their results is given in Sec. IV A.

In the Ericson-Strutinski theory a Gaussian cutoff is assumed for the spin dependence of the level density  $\rho(E, j)$  at a given excitation energy  $E$ . The spin cutoff parameter  $\sigma$ , defined by the expression<sup>10,11</sup>

$$\rho(E, j) = \rho(E, 0) (2j+1) e^{-j(j+1)/2\sigma^2}, \quad (1)$$

characterizes the spin distribution of the residual nucleus. The Gaussian spin cutoff may also be characterized by a moment of inertia  $\mathcal{I}$ . The exponential may be written as  $e^{-E_{\text{rot}}/T}$ , where  $T$  is the nuclear temperature and the rotational energy is given by the usual expression

$$E_{\text{rot}} = \hbar^2 j(j+1)/2\mathcal{I}, \quad (2)$$

with the moment of inertia defined by

$$\mathcal{I} = \hbar^2 \sigma^2 / T. \quad (3)$$

The temperature is defined by the relation

$$1/T = d \ln \rho(E, 0) / dE.$$

The Ericson-Strutinski approach provides a clear physical picture for the cause of the forward-backward peaking. We consider the situation in which the orbital angular momentum is very large compared to the intrinsic spins. Then the total angular-momentum vector is nearly perpendicular to the beam direction. If the only available states of the residual nucleus are also of low spin, the high-spin compound nucleus is forced to decay by emission of a particle with large orbital angular momentum. To conserve the total angular momentum, the angular-momentum vector of this particle must be nearly parallel to the total angular-momentum vector. This means that the final velocity vector is confined essentially to a plane. Averaging over all possible orientations of the total angular-momentum vector, one

\* Research sponsored by the U. S. Atomic Energy Commission under contract with the Union Carbide Corporation.

† Tulane University, New Orleans, Louisiana.

<sup>1</sup> L. Wolfenstein, Phys. Rev. **82**, 690 (1951).

<sup>2</sup> I. Kumabe, Phys. Rev. **106**, 155 (1957).

<sup>3</sup> W. Patzak and H. Vonach, Nucl. Phys. **39**, 263 (1962).

<sup>4</sup> O. N. Kaul, Nucl. Phys. **39**, 325 (1962).

<sup>5</sup> J. Benveniste, G. Merkel, and A. C. Mitchell, Bull. Am. Phys. Soc. **7**, 454 (1962).

<sup>6</sup> W. J. Knox, A. R. Quinton, and C. E. Anderson, Phys. Rev. **120**, 2120 (1960).

<sup>7</sup> C. E. Hunting, Phys. Rev. **123**, 606 (1961).

<sup>8</sup> I. Halpern and V. Strutinski, in *Proceedings of the Second United Nations International Conference on the Peaceful Uses of Atomic Energy, Geneva, 1958* (United Nations, Geneva, 1958), Vol. 15, p. 408.

<sup>9</sup> T. Ericson and V. Strutinski, Nucl. Phys. **8**, 284 (1958); **9**, 689 (1958/59).

<sup>10</sup> C. Bloch, Phys. Rev. **93**, 1094 (1954).

<sup>11</sup> T. Ericson, Advan. Phys. **9**, 435 (1960).

sees that particles must "pile up" in the forward and backward directions because these directions are common to all possible planes of emission. The extreme classical limit has been put on a precise basis by Ericson.<sup>12</sup>

The anisotropy expected in reactions with low angular momentum is small, as mentioned earlier. Nevertheless, it has been observed in  $(p,n)$  reactions.<sup>13</sup> A quantum-mechanical calculation is necessary for analyzing such data properly because of the small angular momenta and because the channel spins cannot be ignored. This kind of computation was carried out for a Gaussian cutoff by Douglas and MacDonald<sup>14</sup>; in essence it amounts to a Hauser-Feshbach calculation<sup>15</sup> adapted to continuous level densities.

Angular-momentum limitation leads to other observable effects. Among these are reduction of particle emission probabilities,<sup>11</sup> enhancement of gamma emission,<sup>16-18</sup> changes in the shape of evaporation spectra and excitation functions,<sup>19</sup> and breakdown of the usual assumption of independence of formation and decay of the compound nucleus.<sup>1,14</sup> The last effect may be stated more precisely as a failure of the cross section to separate into a factor concerned only with formation of the compound nucleus times another factor dealing only with the relative probability of decay into a given channel.

In our experiments three low- $Z$  targets (oxygen, sodium, and aluminum) were bombarded with 27-MeV  $^{14}\text{N}$  ions. The present work is an extension of earlier work on oxygen<sup>20</sup> and aluminum.<sup>21</sup> Energy spectra of alpha particles were obtained at about 20 angles from 0 to 165° (lab). Excitation energies in the compound nucleus were about 40 MeV. Angular momenta as high as  $12\hbar$  are important in the entrance channel, as may be seen from the transmission coefficients plotted in Fig. 1.

The over-all energy spread in the entrance channel was appreciable due to target thickness and beam-energy spread ( $\approx 1$  MeV). Usually a large number of final states contributed to each measured cross section. Consequently, statistical fluctuations<sup>11,22</sup> in the measured cross sections were averaged out and symmetry about 90° was expected. The angular distributions are, in fact, symmetric about 90° within experimental error. The measured angular distributions are strongly peaked forward and backward, indicating immediately that

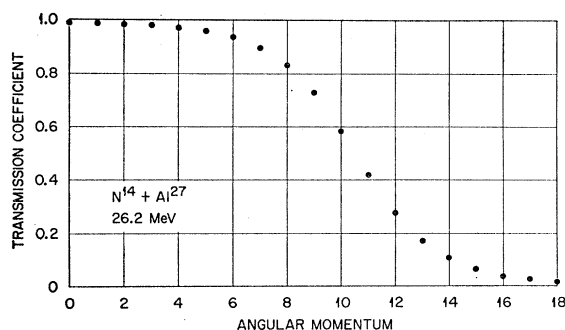


FIG. 1. Transmission coefficients as a function of orbital angular momentum for 26.2-MeV nitrogen-14 on aluminum-27. The optical potential used to obtain these numbers is given in Appendix 1.

the number of high-spin levels in the residual nucleus must be severely limited. The data also demonstrate the breakdown of the independence assumption.

The semiclassical theory was programmed in FORTRAN and the spin cutoff parameters  $\sigma$  were obtained for the various final nuclei. The variation of level density with excitation energy was determined: fits to two forms of the Fermi-gas level density were obtained. A partial account of the analysis was given as a conference report.<sup>23</sup> The quantum-mechanical theory<sup>14</sup> was recently programmed in FORTRAN; a description of the program and its application to some of the present experimental data will be given in another paper.<sup>24</sup>

The Gaussian approximation to the spin cutoff factor is used throughout the present analysis. It predicts a finite probability for arbitrarily large values of spin, but of course  $j$  cannot exceed  $j_{\text{max}}$ , the value the angular momentum would have if all the excitation energy of the nucleus were in the form of rotational energy. Breakdown of the Gaussian form is to be expected near this limit. More accurate approximations to the cutoff factor exist,<sup>10,25</sup> but the Gaussian is probably adequate for the present analysis, since  $j_{\text{max}}$  is of the order of 15 to 20, as computed from (2) using the rigid-body moment of inertia. The entrance-channel transmission coefficients are quite small for such large angular momenta.

## II. EXPERIMENTAL METHOD

The beam of triply-charged  $^{14}\text{N}$  ions was accelerated by the Oak Ridge 63-in. Cyclotron. The target was placed at the center of a 24-in. diameter scattering

<sup>12</sup> T. Ericson, Nucl. Phys. **17**, 250 (1960).

<sup>13</sup> D. L. Allan, Nucl. Phys. **10**, 348 (1959).

<sup>14</sup> A. C. Douglas and N. MacDonald, Nucl. Phys. **13**, 382 (1959).

<sup>15</sup> W. Hauser and H. Feshbach, Phys. Rev. **87**, 366 (1952).

<sup>16</sup> G. N. Flerov, in *Proceedings of the Second United Nations International Conference on the Peaceful Uses of Atomic Energy, Geneva, 1958* (United Nations, Geneva, 1958), Vol. 14, p. 151.

<sup>17</sup> J. F. Mollenauer, Phys. Rev. **127**, 867 (1962).

<sup>18</sup> J. R. Grover, Phys. Rev. **123**, 267 (1961); **127**, 2142 (1962).

<sup>19</sup> T. Kammuri, Progr. Theoret. Phys. (Kyoto) **25**, 235 (1961); **28**, 754 (1962).

<sup>20</sup> M. L. Halbert and A. Zucker, Phys. Rev. **114**, 132 (1959).

<sup>21</sup> A. Zucker, Nucl. Phys. **6**, 420 (1958).

<sup>22</sup> T. Ericson, Ann. Phys. (N. Y.) **23**, 390 (1963).

<sup>23</sup> M. L. Halbert and F. E. Durham, in *Proceedings of the Third Conference on Reactions Between Complex Nuclei*, edited by A. Ghiorso, R. M. Diamond, and H. E. Conzett (University of California Press, Berkeley, 1963), p. 223.

<sup>24</sup> H. F. Bowsher, (unpublished). A preliminary account is given in an Oak Ridge National Laboratory technical memorandum, ORNL-TM-971 (unpublished).

<sup>25</sup> D. W. Lang, in *Proceedings of the Third Conference on Reactions Between Complex Nuclei*, edited by A. Ghiorso, R. M. Diamond, and H. E. Conzett (University of California Press, Berkeley, 1963), p. 248.

TABLE I. List of reactions and related quantities. All energies are in MeV. The quantity  $I_0$  is the incident orbital angular momentum for which the transmission coefficient is  $\approx 0.5$ , according to optical-model computations.

Reaction	Target	Incident beam energy	Mean energy in target	$Q$	Compound nucleus	Excitation energy of compound nucleus	$I_0$	Maximum alpha energy	
								c.m. system	lab system, $0^\circ$
$^{16}\text{O}(^{14}\text{N},\alpha)^{26}\text{Al}$	Copper oxide	27.9	27.2	7.904	$^{30}\text{P}$	32.8	11.9	22.4	32.6
$^{16}\text{O}(^{14}\text{N},\alpha)^{26}\text{Al}$	Copper oxide	24.7	24.0	7.904	$^{30}\text{P}$	31.1	10.2	20.7	29.8
$^{23}\text{Na}(^{14}\text{N},\alpha)^{33}\text{S}$	Sodium bromide	27.3	26.7	17.495	$^{37}\text{Ar}$	40.9	11.7	34.1	43.0
$^{27}\text{Al}(^{14}\text{N},\alpha)^{37}\text{Ar}$	Aluminum	27.4	26.6	14.190	$^{41}\text{Ca}$	38.3	10.5	31.7	39.6

chamber. Charged particles produced by reactions in the target were detected by a silicon surface-barrier diode mounted on a movable arm. Spectra were obtained at angles from  $0$  to  $165^\circ$  with respect to the beam direction. Pulses from the diode were amplified by a charge-sensitive preamplifier, a linear amplifier, and then were sorted by a 256-channel analyzer. Spectra obtained in this way were later converted to center-of-mass cross sections by a high-speed digital computer.

A list of the reactions studied and of various associated information is given in Table I.

### A. Targets

The oxygen reaction was studied with a copper oxide target, prepared by baking a  $6 \text{ mg/cm}^2$  copper foil at  $250^\circ\text{C}$  for about an hour. The increase of weight corresponded to  $0.10 \text{ mg/cm}^2$  of oxygen on each side. Since the beam energy was well below the Coulomb barrier for copper, essentially no reactions occurred in the copper. No reactions took place in the oxygen on the back of the foil because the beam lost practically all of its energy as it went through the copper.

The sodium target was a  $0.29 \text{ mg/cm}^2$  layer of NaBr vacuum evaporated onto a  $7 \text{ mg/cm}^2$  nickel foil. As with copper, no reactions occurred in the bromine or the nickel.

Two aluminum targets were used. One was a commercial foil  $0.17 \text{ mg/cm}^2$  thick. The other, prepared by evaporation onto a  $7 \text{ mg/cm}^2$  nickel backing, was about  $0.16 \text{ mg/cm}^2$  thick.

To allow measurements near  $90^\circ$ , the targets were tilted at an angle of  $40^\circ$  to the beam. The effective target thickness was typically about  $1.5 \text{ MeV}$ . When the data were converted to the center-of-mass system, all reactions were assumed to have occurred halfway through the target. A more refined estimate of the mean energy of reaction, taking into account the variation of cross section with energy, did not give a significantly different result.

### B. Detector

Most of the data were obtained with an  $n$ -type silicon surface-barrier diode especially selected for high resistivity ( $2500 \Omega\text{-cm}$ ) and ability to operate at high bias voltage without generating noise. With this device, the

sensitive depth was sufficient to stop 40-MeV alpha particles with 600 V bias. This was adequate for all targets except sodium. Alphas emitted near  $0^\circ$  from  $^{23}\text{Na}$  have energies as high as 43 MeV. An absorber was placed in front of the counter for measurements in the forward direction.

In this experiment the particles of interest were the medium- to high-energy alphas. The detector is sensitive to any charged particle, but proton and deuteron pulses could be completely excluded from the region of interest by adjusting the bias on the counter. The method was simply to make the sensitive depth just a little greater than the range of the maximum-energy alpha particles for the angle and target under study. Then no proton could give up more than about  $\frac{1}{4}$  of the maximum alpha energy, and a definite cutoff of the proton continuum was observed. This is illustrated in Fig. 2. For this spectrum the sensitive depth was set equal to the range of a 36-MeV alpha particle, which is almost the same as the range of a 9-MeV proton. A sharp drop in counting rate is evident at 9 MeV, due to the proton cutoff. The

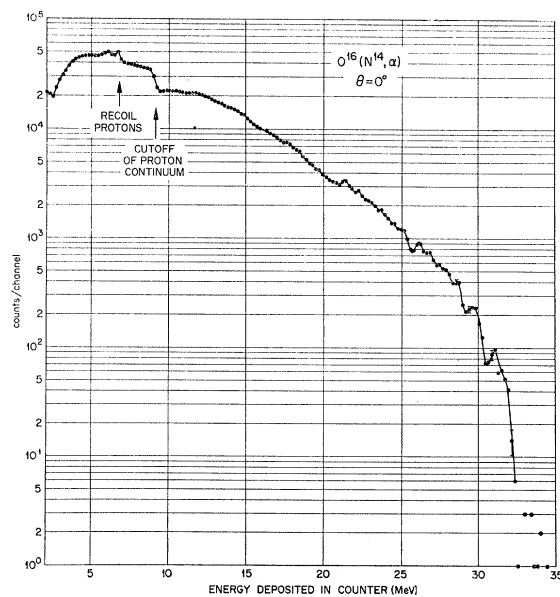


Fig. 2. Zero-degree spectrum of alpha particles from the bombardment of copper oxide by nitrogen-14 ions with mean energy 27.2 MeV.

peak labeled "recoil protons" is due to hydrogen impurity in the target.

The energy of the ground-state alpha particles was a strong function of angle. To obtain the correct sensitive depth, the detector bias was varied from 615 V for the zero-degree alphas from the NaBr target to 7 V for the oxygen reaction at  $165^\circ$ . The bias required for each run was determined from a nomograph<sup>26</sup> based on the relation between bias and depletion depth predicted by the Schottky theory, which assumes that a sharp boundary exists between the totally depleted and undepleted regions of the silicon.<sup>27</sup> The validity of this relation was previously established for this counter from 2 to 500 V bias.<sup>28</sup> A direct check on the sensitive depth was available in each spectrum since the proton cutoff always showed up clearly.

The maximum energy for deuterons is somewhat greater than for protons. In Fig. 2, the deuteron cutoff should occur at 11 MeV. There is a slight drop in counting rate just above that energy, but evidently few deuterons are present. The spectra from the other targets also show very few deuterons. No evidence for a triton cutoff could be detected. This agrees with measurements with a  $(dE/dx, E)$  particle selector in reactions of  $^{14}\text{N}$  on oxygen<sup>20</sup> and aluminum<sup>21</sup> which showed that tritons are very rare.

Heavier ions were present in appreciable numbers, mostly  $^{14}\text{N}$  scattered by the target and its backing. None of these particles entered the counter at forward angles because a nickel foil sufficiently thick to stop the direct beam (7 to 12 mg/cm<sup>2</sup>) was placed just beyond the target. At backward angles, it was necessary to place several mg/cm<sup>2</sup> of absorber in front of the counter to stop scattered  $^{14}\text{N}$  and products of transfer reactions. Corrections were made for the energy loss of the alpha particles in this absorber or the target backing.

### C. Energy Calibration

Accurate calibration of the energy scale was important in this experiment. The counting rate varies rapidly with channel number, so that small discrepancies in energy scale can cause large errors. The spectra are usually quite featureless and consequently the conversion gain (MeV per channel) cannot be determined from the spectra themselves.

The required calibration can be broken into two parts: first, measurement of the departure from linearity of the detector and the electronics, and second, determination of the conversion gain. The linearity of the preamplifier, and pulse-height analyzer was measured by a precision pulser which injected charge at the preampli-

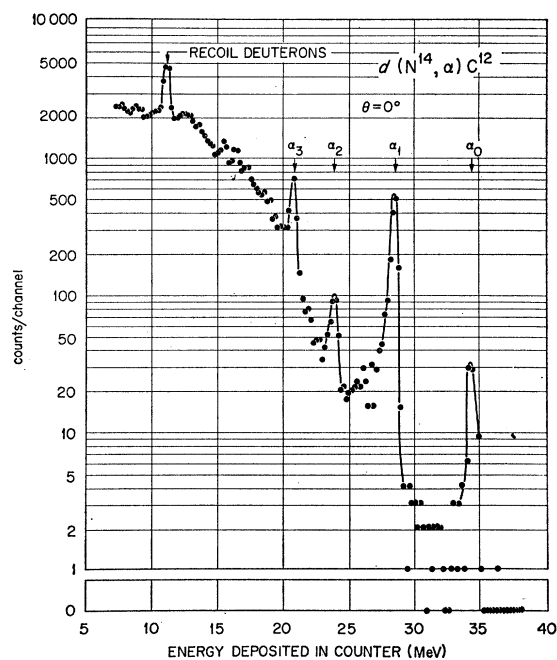


FIG. 3. Zero-degree spectrum of alpha particles from the bombardment of deuterium by 27-MeV nitrogen-14. In the analysis it was assumed that the peaks labeled  $\alpha_0$ ,  $\alpha_1$ ,  $\alpha_2$ , and  $\alpha_3$  are due to transitions to the ground, first, second, and third excited states of  $^{12}\text{C}$ , respectively. The peak at about 11 MeV was assumed to be due to deuterons projected forward by elastic collisions with the nitrogen ions.

fier input. The differential nonlinearity in the region of interest was less than 2%; a correction for the measured nonlinearity was incorporated in the data reduction.

The response of the detector used in this work was checked for linearity with alpha particles from 20 to 34 MeV obtained from the reaction  $d(^{14}\text{N}, \alpha)^{12}\text{C}$  at forward angles, corresponding to the ground state and first three excited states of  $^{12}\text{C}$ . A special gas cell containing deuterium gas at a pressure of 5 cm Hg was used. The  $^{14}\text{N}$  beam entered the gas through an 0.65 mg/cm<sup>2</sup> nickel foil and stopped in an exit foil plus beam stopper combination totaling about 8 mg/cm<sup>2</sup> of nickel. A zero-degree spectrum is shown in Fig. 3, and the response curve calculated from this run and another at  $10^\circ$  is given in Fig. 4. Figure 4 also includes data from the deuteron recoil peak indicated in Fig. 3. Within the accuracy of this measurement, the detector is linear.

The results just presented are also useful for the second part of the calibration problem. Values of the conversion gain can be derived from the data plotted in Fig. 4. This method of calibration was, in fact, used for about half the data. In the other runs, the conversion gain was determined as a byproduct of the beam-energy measurements described in Sec. E. The deuterium method depends somewhat on the accuracy of the beam-energy measurement since the  $^{14}\text{N}$  bombarding energy must be known in order to calculate the energies of the alphas produced in the  $d(^{14}\text{N}, \alpha)^{12}\text{C}$  reaction, but

<sup>26</sup> J. L. Blankenship, I.R.E. Trans. Nucl. Sci. **7**, 190 (1960).

<sup>27</sup> See for example J. Bardeen, in *Handbook of Physics*, edited by E. V. Condon and H. Odishaw (McGraw-Hill Book Company, Inc., New York, 1958), Part 8, especially the section beginning on p. 8-60.

<sup>28</sup> M. L. Halbert, *Nuclear Electronics* (International Atomic Energy Agency, Vienna, 1962), Vol. I, p. 403.

it is less sensitive to error in the beam energy because the  $Q$  of the deuterium reaction is large and the  $^{14}\text{N}$  kinetic energy contributes only a portion of the final alpha-particle energy. Unfortunately, this advantage is offset by the uncertainty ( $\approx 0.1$  MeV) in the energy loss of the  $^{14}\text{N}$  as it goes through the entrance foil of the gas target.

The assignment of conversion gain is thought to be reliable to about 1%. For the most energetic alphas, this represents an uncertainty of 0.3 to 0.4 MeV in particle energy, and a similar possible error in the residual-nucleus excitation energy to which a particular alpha particle corresponds. A check of this estimate was made by bombardment of a carbon target, since the ground-state transition for  $^{12}\text{C}(^{14}\text{N}, \alpha)^{22}\text{Na}$  stands out clearly. The apparent energy of the ground-state peak was within 0.2 MeV of the energy calculated from kinematics, which is consistent with our estimate of the uncertainty.

#### D. Beam Intensity

The  $^{14}\text{N}$  beam was always stopped in a foil just beyond the target. The target and beam stopper were insulated from ground so that the beam current could be monitored and integrated with a chopper amplifier. Usually the beam current was between 0.02 and 0.05  $\mu\text{A}$  (triply charged ions). No difficulty due to electron loss from the target was experienced because the apparatus was close to the cyclotron and the stray magnetic field was sufficient to suppress emission of secondaries from the target.

#### E. Beam Energy

Data from the oxygen target were obtained with an incident-beam energy of 27.9 MeV, while the sodium and aluminum data were taken at 27.3 and 27.4 MeV. This variation seemed to be due to a long-term change in the operating conditions of the cyclotron. The short-term stability was adequate to insure that all data for a given target were obtained at the same bombarding energy to within 0.1 MeV. Allowance for energy loss in penetrating to the center of each target gives the mean bombarding energies listed in Table I.

One set of data for  $^{16}\text{O}$  was obtained at reduced bombarding energy. The incident beam was degraded with an 0.67 mg/cm<sup>2</sup> nickel foil placed just in front of the target. The measured energy with this foil was  $3.2 \pm 0.3$  MeV lower than without it. The mean energy in the target was taken as 24.0 MeV for these data.

The beam energy was measured by comparing the pulse height in a surface-barrier diode of  $^{234}\text{U}$  alphas with that for  $^{14}\text{N}$  ions scattered through  $90^\circ$  by a thin gold foil. The comparisons were actually made by means of a precision pulser, with the pulse-height analyzer used merely as a null instrument; details are given elsewhere.<sup>29</sup> The method is accurate to about  $\pm 0.1$  MeV.

<sup>29</sup> M. L. Halbert and A. Zucker, Phys. Rev. **121**, 236 (1961).

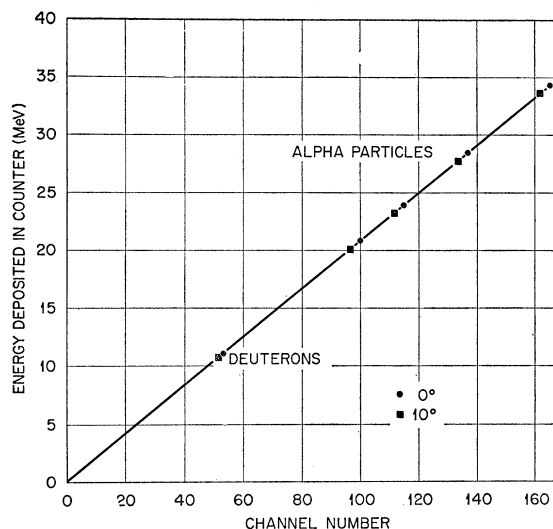


FIG. 4. Pulse-height response of the surface-barrier detector for alpha particles and deuterons. The  $0^\circ$  points were obtained from Fig. 3, while a similar spectrum taken at  $10^\circ$  (lab) provided the other points.

The  $^{14}\text{N}$  scattering peak provides the calibration of conversion gain (MeV/channel) mentioned earlier.

#### F. Angular Resolution and Accuracy

The angular resolution in this experiment was determined principally by the acceptance of the counter, which was approximately a cone of half-angle  $1.4^\circ$  for most of the data. The finite size of the beam spot corresponded to about  $1^\circ$ ; divergence of the beam was negligible in comparison. The over-all resolution was about  $1.7^\circ$ . In the center-of-mass system of the final nuclei the resolution was typically  $2.0^\circ$  at forward angles and  $1.5^\circ$  at back angles. The major part of the 27.2-MeV data from the oxygen target was obtained with a collimator of half-angle  $1.0^\circ$  (lab), so that the over-all resolution in this case varied between  $1.6$  and  $1.2^\circ$  in the center-of-mass system.

To take full advantage of the angular resolution, it was essential to make accurate determinations of the angle settings of the counter. The mechanical design of the chamber made it possible to measure rotation about the center to  $\pm 0.1^\circ$ . A check of chamber positioning was made before each series of runs by allowing the beam to char a piece of masking tape placed on the target holder to verify that the beam actually passed through the center of rotation. The beam direction was then determined by measuring elastic scattering from a thin aluminum target on both sides of the beam. Matching of the counting rate and pulse height on the two sides permitted the zero angle to be assigned with an accuracy of  $\pm 0.2^\circ$ .

## III. EXPERIMENTAL DATA

For each target the raw data consisted of pulse-height spectra similar to Fig. 2 obtained at various angles from 0 to 165° (lab). These data were converted, channel by channel, to center-of-mass differential cross sections with an automatic computer. Corrections for nonlinearity of amplifier response and for energy loss of the alpha particles in absorber between target and detector were incorporated in the program used. Further operations were performed by another program which averaged the center-of-mass differential cross sections over a given interval of excitation energy (usually chosen as 1 MeV). The program then fit the averaged angular distributions for each excitation energy with Legendre polynomials by the method of least squares.

## A. Oxygen

Figure 5 is a zero-degree spectrum of alpha particles from the oxygen target after conversion to the center-of-mass system of  $\alpha + {}^{26}\text{Al}$ . The original data are those of Fig. 2. The structure evident in this spectrum was noted previously.<sup>20</sup> Since data at different angles and different bombarding energies show the peaks at the same excitation energy after transformation to the center-of-mass system, the structure is thought to be due to isolated states or groups of states in the residual nucleus. The rapid increase of the cross section with excitation energy is characteristic of the statistical decay of a compound nucleus.

Complete angular distributions were obtained at two energies, 27.2 and 24.0 MeV. The cross sections averaged over 1-MeV bands in excitation energy are given in Figs. 6 and 7. The smooth curves are least-squares fits with  $c_0 + c_2 P_2(\cos \theta) + c_4 P_4(\cos \theta) + c_6 P_6(\cos \theta)$ , where  $\theta$  is the center-of-mass angle. Fits with a  $P_8$  term were not significantly better for these data or the data from the sodium and aluminum targets. Points at large angles are missing from the curves at high excitation energy

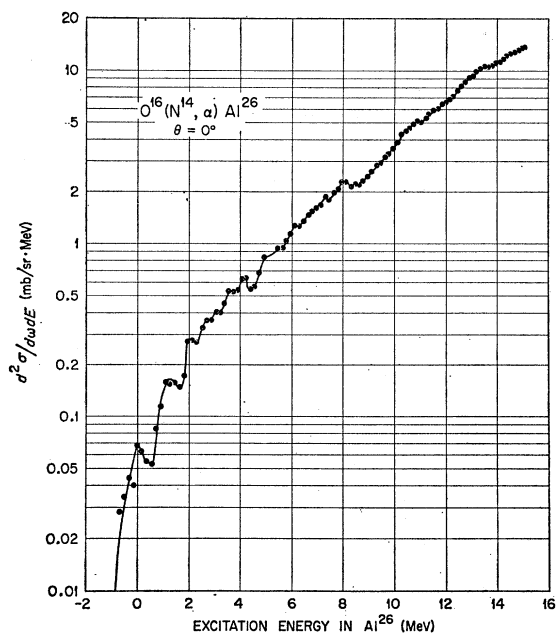


Fig. 5. Center-of-mass differential cross section at 0° for alpha particles from oxygen.

because the corresponding alpha-particle energy was below the proton cutoff.

## B. Sodium

Examples of two zero-degree spectra of alpha particles from bombardment of NaBr are shown in Fig. 8. These have been converted to the  $\alpha + {}^{38}\text{S}$  center-of-mass system.

It is clear that transitions to low-lying states of the residual nucleus are rare; no transitions at all to states below 5 MeV excitation were detected. This is a result of the severe competition with transitions to levels of high excitation, where the level density is much higher

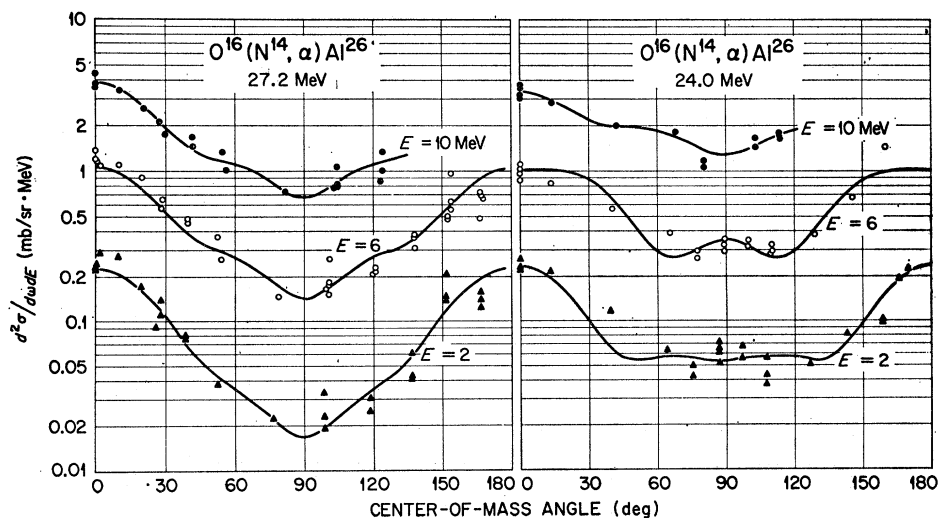


Fig. 6. Average center-of-mass differential cross sections as a function of angle for alpha particles from oxygen for residual-nucleus excitation energies of 2, 6, and 10 MeV.

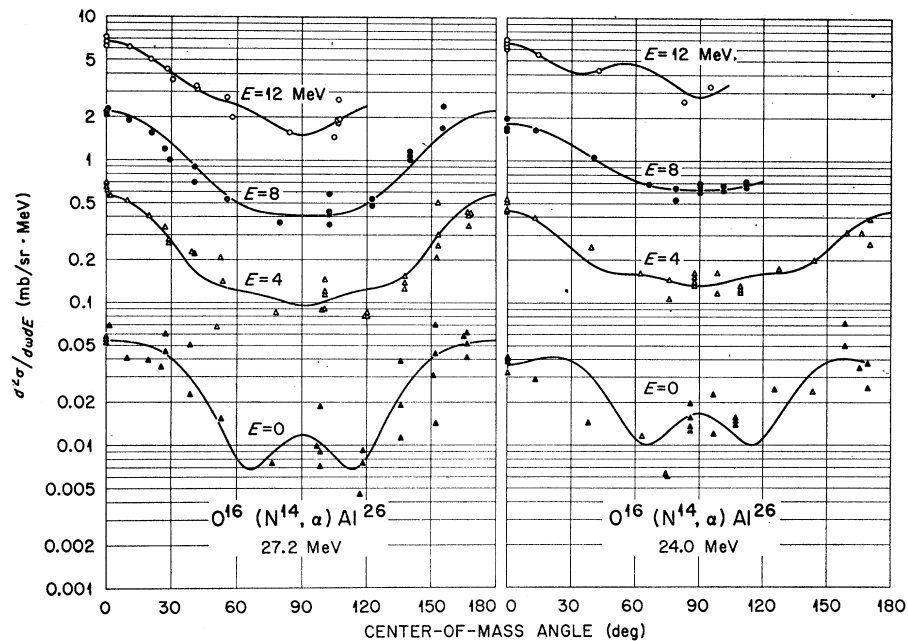


FIG. 7. Average center-of-mass differential cross sections as a function of angle for alpha particles from oxygen for residual-nucleus excitation energies of 0, 4, 8, and 12 MeV.

and confirms the statistical nature of the decay of the compound system.

Buildup of a black spot on the target was observed during bombardment, and a check was made for carbon contamination. The open circles in Fig. 8 were obtained after about 15 h bombardment of the target. The heavy points of Fig. 8 were obtained immediately afterward, with the target moved to expose a fresh spot to the beam. The arrow indicates the calculated position of the ground-state transition for  $^{14}\text{N}$  on  $^{12}\text{C}$ ; it points directly

at a peak in the upper curve. There is also clearly an excess of particles at excitation energies above the arrow. Evidently carbon buildup is appreciable. In contrast, the spectra from oxygen showed no evidence of carbon contamination.

Figures 9 and 10 give the differential cross sections averaged over 1-MeV bands in  $^{38}\text{S}$  excitation energy. All data subject to contamination by alphas from carbon impurity were rejected, which accounts for the lack of points at forward angles in some of the curves. Fortu-

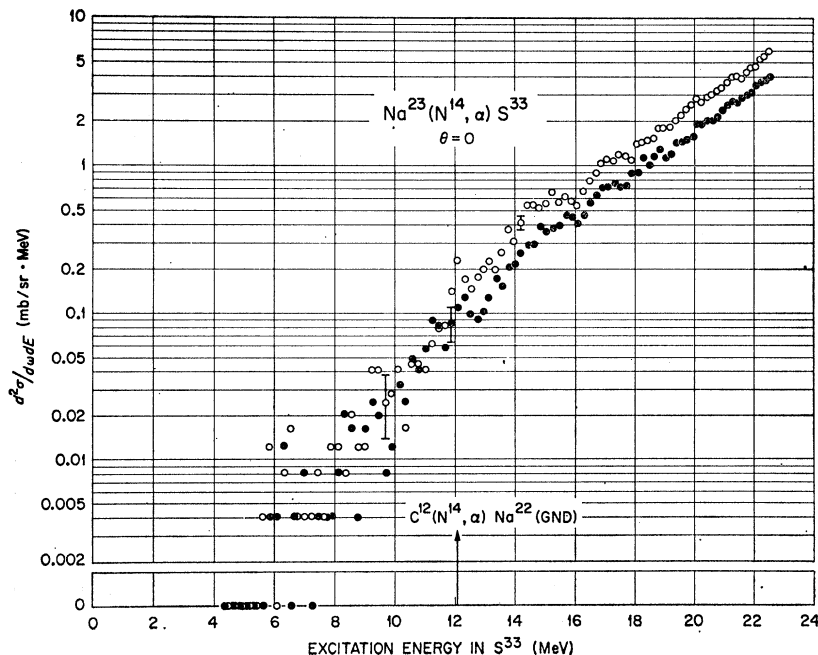


FIG. 8. Center-of-mass differential cross sections at  $0^\circ$  for alpha particles from sodium. These data demonstrate the effect of carbon buildup during bombardment. The closed circles were obtained with a fresh spot on the target, while the open circles were obtained after a long bombardment on another spot. The arrow indicates the energy at which ground-state alpha particles from carbon should appear.

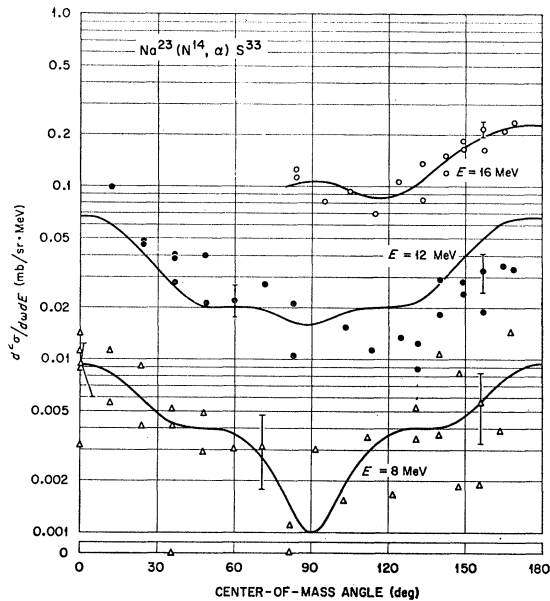


FIG. 9. Average center-of-mass differential cross sections as a function of angle for alpha particles from sodium for residual-nucleus excitation energies of 8, 12, and 16 MeV.

nately, the maximum energy of these unwanted alpha particles decreases rapidly with angle because of the large center-of-mass motion, and beyond  $90^\circ$  none of the potentially useful data had to be discarded. Statistical uncertainties are large in the data for low excitation energy because these events were so rare. As before, the smooth curves are least-squares fits with even-order Legendre polynomials up to  $P_6$ .

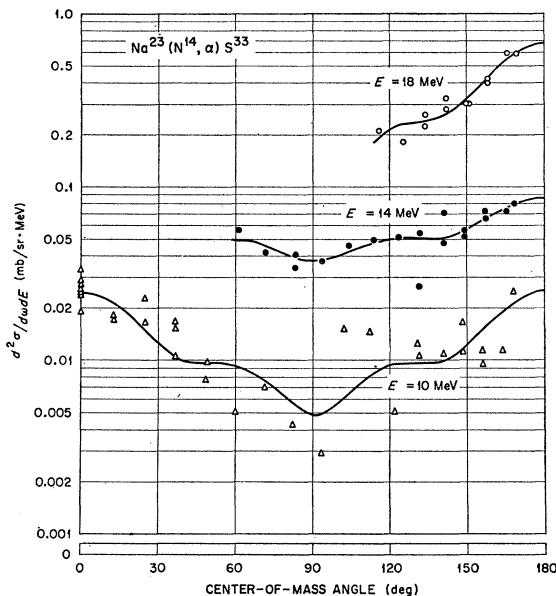


FIG. 10. Average center-of-mass differential cross sections as a function of angle for alpha particles from sodium for residual-nucleus excitation energies of 10, 14, and 18 MeV.

### C. Aluminum

As with the sodium data, transitions to the lowest states of the residual nucleus were not detected. This may be seen in Fig. 11, a zero-degree spectrum taken with the evaporated target. The arrow marks the energy for the  $^{12}\text{C}(^{14}\text{N}, \alpha)^{22}\text{Na}$  ground-state transition. The absence of a peak there indicates that carbon contamination of this target was not serious. In contrast, the data obtained with the commercially obtained foil showed a strong peak at that energy even when a completely fresh spot was bombarded. Accordingly, the data from this target above the threshold for alpha particles from carbon were discarded. All the data at forward angles were obtained with the freshly prepared evaporated target, so that the contamination problem was circumvented.

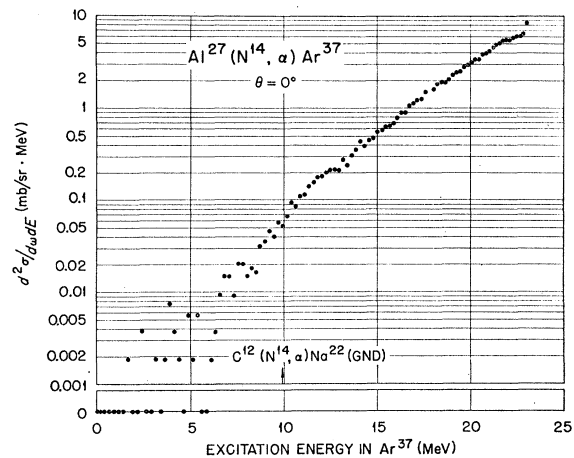


FIG. 11. Center-of-mass differential cross section at  $0^\circ$  for alpha particles from the evaporated aluminum target. The arrow indicates the energy at which ground-state alpha particles from carbon would appear.

The differential cross sections, averaged over 2-MeV bands in excitation of the residual nucleus, are shown in Fig. 12. The agreement between the data from the two targets was good wherever comparisons could be made. Data points at large angles are missing from the two highest curves because the corresponding particles were below the proton cutoff energy. The smooth curves again are least-squares fits with  $P_0$ ,  $P_2$ ,  $P_4$ , and  $P_6$ .

## IV. ANALYSIS OF DATA

### A. Theoretical Considerations

The semiclassical expression<sup>11</sup> for the statistical decay of a compound nucleus into exit channel  $\nu$  may be written as an expansion in even-order Legendre polynomials

$$\frac{d^2\sigma(i \rightarrow \nu)}{d\omega dE} = \sum_k c_{2k}(i, \nu) P_{2k}(\cos\theta). \quad (4)$$

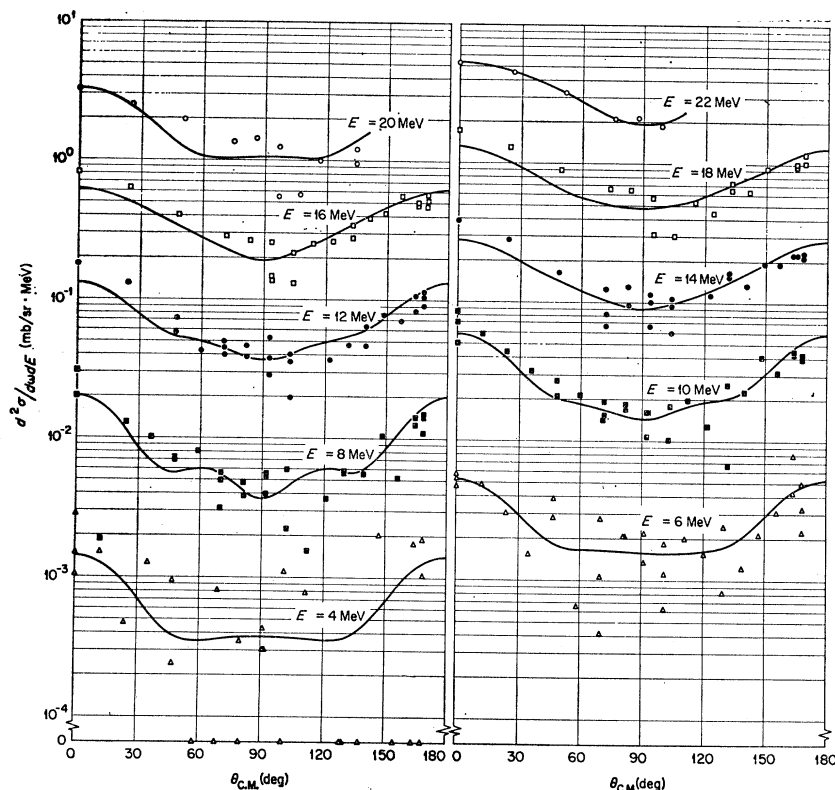


FIG. 12. Average center-of-mass differential cross sections for alpha particles from aluminum for various residual-nucleus excitation energies.

Here  $i$  designates the entrance channel and  $\theta$  is the center-of-mass angle of emission. The  $c_{2k}$  are given by

$$c_{2k}(i, \nu) = \pi \lambda_i^2 f(k) \sum_I (2I+1) T_I^i \frac{F^\nu(I, k, E)}{\sum_{\nu'} \int dE F^{\nu'}(I, 0, E)}, \quad (5)$$

with

$$F^\nu(I, k, E) = (2s_\nu + 1) \rho_\nu(E, 0) \sum_l (2l+1) T_l^\nu \times \exp\left[-\frac{(I + \frac{1}{2})^2 + (l + \frac{1}{2})^2}{2\sigma_\nu^2}\right] j_{2k}\left[\frac{i(I + \frac{1}{2})(l + \frac{1}{2})}{\sigma_\nu^2}\right], \quad (6)$$

and

$$f(k) = ((-1)^k / 4\pi) (4k+1) [(2k)! / (2^k k!)^2]^2. \quad (7)$$

The quantities  $\sigma_\nu$  and  $\rho_\nu(E, 0)$  are the spin cutoff parameter and energy dependence of the level density of the residual nucleus in channel  $\nu$ , as defined in (1). The other symbols are defined as follows:

$\lambda$  = de Broglie wavelength

$I$  = orbital angular momentum in channel  $i$

$l$  = orbital angular momentum in channel  $\nu$

$T$  = transmission coefficient

$s_\nu$  = spin of emitted particle in channel  $\nu$

$j_{2k}$  = spherical Bessel function of order  $2k$ .

This expression differs slightly from Eq. (5.26) of

Ericson<sup>11</sup> in that  $I + \frac{1}{2}$  and  $l + \frac{1}{2}$  are substituted for  $I$  and  $l$ , and the sums over  $I$  and  $l$  replace integrals. Comments on the evaluation of (5), together with a list of the parameters chosen, are given in Appendix 1. Approximations to the Ericson-Strutinski formula are discussed in Appendix 2.

The semiclassical approximation is valid if

$$\max(\bar{I}, \bar{l}) \lesssim 2\sigma^2, \quad (8)$$

where  $\bar{I}$  and  $\bar{l}$  represent effective values of orbital angular momentum.<sup>11</sup> In these experiments,  $\bar{I}$  is always the larger of the two. Judging from Fig. 1,  $T_I$  for  $I$  above about 15 is not important in the  $N^{14} + Al^{27}$  system. Thus values of  $\sigma \lesssim 2.7$  may be safely handled with this approximation. Estimates of the safe values of  $\sigma$  for the other targets are similar.

In the limit of very strong cutoff ( $\sigma_\nu \rightarrow 0$ ), it is easy to show that the angular distribution approaches  $1/\sin\theta$ , an extreme demonstration of the forward-backward peaking.<sup>11,12</sup> The opposite extreme of unlimited spin values ( $\sigma_\nu \rightarrow \infty$ ) leads to isotropy because  $j_{2k}(0) = 0$  for all  $k > 0$ . Furthermore, the  $I$  dependence of  $F^\nu(I, 0, E)$  disappears, and  $c_0(i, \nu)$  can be broken into one factor describing the formation of the compound system and another referring only to its decay. The dependence of the latter factor on the exit-channel energy is contained in  $\rho_\nu(E, 0)$  and  $\sum_l (2l+1) T_l^\nu$ . If we identify the latter as  $\sigma_c(\epsilon) / (\pi \lambda_\nu^2)$ , where  $\sigma_c(\epsilon)$  is the cross section for forming the compound nucleus by the inverse reaction at channel

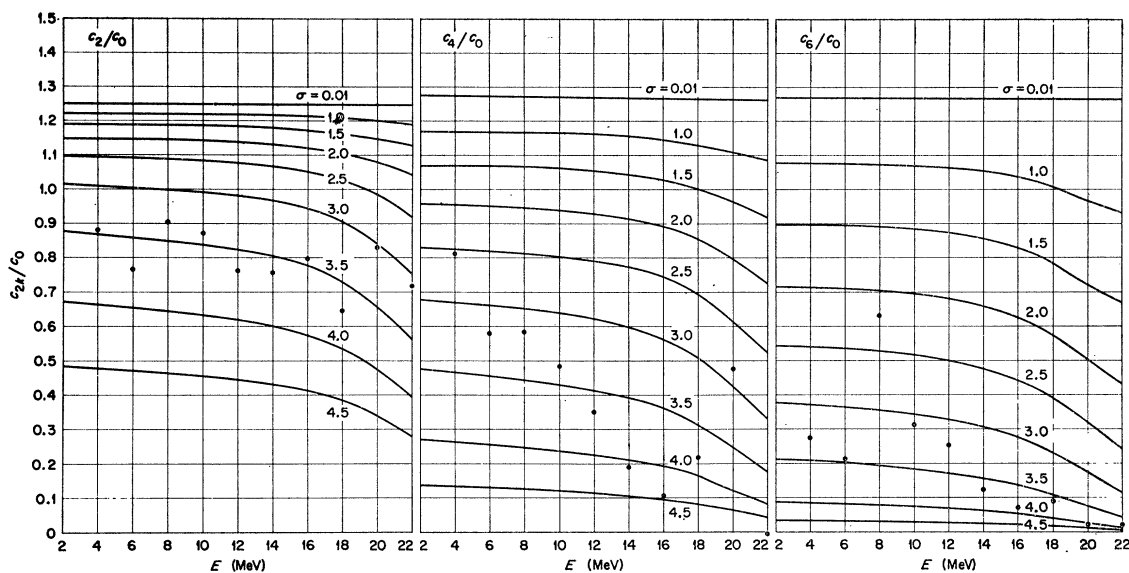


FIG. 13. Legendre coefficients as a function of residual-nucleus excitation energy. The points are from the least-squares fits to the measured angular distributions of alpha particles from aluminum. The curves were calculated from the Ericson-Strutinski theory with the spin cutoff parameter  $\sigma$  held constant.

energy  $\epsilon$ , we obtain a familiar result<sup>30</sup> for the energy spectrum of emitted particles

$$N(\epsilon) \approx \epsilon \sigma_c(\epsilon) \rho_\nu(E, 0). \quad (9)$$

In the general case, when spin limitation does exist, the separation into formation and decay factors cannot be made.

### B. Determination of Spin Cutoff Parameter

For each value of  $E$ , different sets of Legendre coefficients  $c_0, c_2, \dots$  were generated by inserting various values of  $\sigma$  into (6). These were compared with the corresponding coefficients of the least-squares fits to the experimental data so that the value of  $\sigma$  giving the best fit could be selected.

The method of comparison is illustrated in Fig. 13 for the reaction  $^{27}\text{Al}(^{14}\text{N}, \alpha)^{37}\text{Ar}$ . The smooth curves are the theoretical values of  $c_2/c_0, c_4/c_0$ , and  $c_6/c_0$  predicted for the indicated choices of  $\sigma$ . The same value of  $\sigma$  was used for all exit channels. The choice of the other parameters is discussed in Appendix 1. The curves are presented as a function of excitation energy in  $^{37}\text{Ar}$  in order to emphasize the requirement of continuity of  $\sigma$  with  $E$  in the selection of the best over-all value of  $\sigma$ .

The dots are the experimental least-squares values. Although the scatter of the points is disappointingly large, there is little doubt that a value of  $\sigma$  close to 3.5 gives the best fit. According to the criterion (8), this is sufficiently large to validate the semiclassical approximation. This method of analysis provides a strong check on the validity of the theoretical formula, since

actually three values of  $\sigma$  are determined independently and they must be consistent. At the same time it is a more sensitive way to determine  $\sigma$  than direct comparison of the experimental and theoretical angular distributions. This point is illustrated in Fig. 14.

In the calculations for Figs. 13 and 14,  $\sigma$  was held constant. Actually,  $\sigma$  is expected<sup>10</sup> to vary as the fourth root of  $E$ . Since the nuclear temperature varies roughly as the square root of  $E$ , the moment of inertia defined

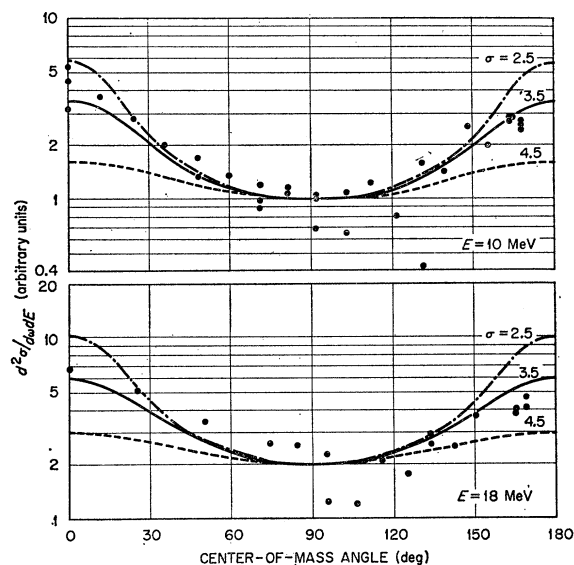


FIG. 14. Angular distributions of alpha particles from aluminum for residual-nucleus excitation energies of 10 and 18 MeV. The points are the measured cross sections taken from Fig. 12, while the curves are calculated from the Ericson-Strutinski theory with the spin cutoff parameter set equal to 2.5, 3.5, or 4.5.

<sup>30</sup> J. M. Blatt and V. F. Weisskopf, *Theoretical Nuclear Physics* (John Wiley & Sons, Inc., New York, 1952), p. 367.

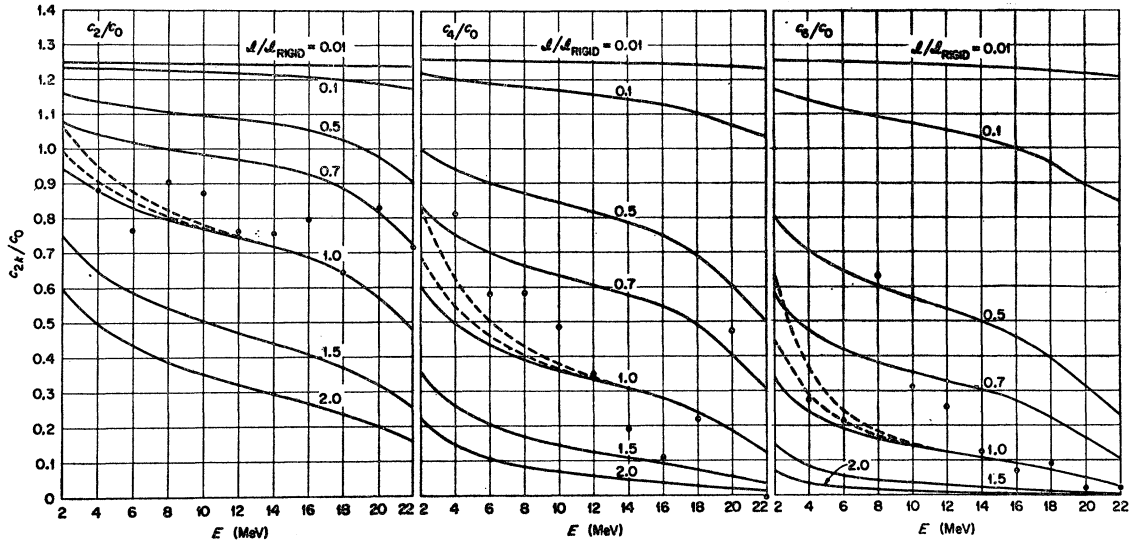


FIG. 15. Legendre coefficients as a function of residual nucleus excitation energy. The points are from the least-squares fits to the measured angular distributions of alpha particles from aluminum. The solid curves were calculated from the Ericson-Strutinski theory with the moment of inertia  $\mathcal{I}$  held constant. The dashed curves show the effect of varying  $q$  in Eq. (11); the upper curves are for  $q=1.0$ , while the lower ones are for  $q=0.5$ .

by (3) is expected to be more nearly independent of energy than is  $\sigma$ . We therefore repeated the calculations with the moment of inertia held constant. We express  $\mathcal{I}$  in units of  $\mathcal{I}_{\text{rigid}}$ , the rigid-body moment, which has the advantage of expressing results in a mass-independent way.<sup>31</sup> In our work the reference body is a rigid sphere of radius  $1.20 \times 10^{-13} A^{1/3}$  cm and mass equal to that of the nucleus under consideration, so that

$$\mathcal{I}_{\text{rigid}}/\hbar^2 = (A^{5/3}/72.6)\text{MeV}^{-1}, \quad (10)$$

where  $A$  is the mass number of the residual nucleus.

Figure 15 shows  $c_{2k}/c_0$  for various constant values of  $\mathcal{I}/\mathcal{I}_{\text{rigid}}$  for the  $^{27}\text{Al}(^{14}\text{N},\alpha)^{37}\text{Ar}$  reaction. The same experimental points are plotted. Admitting again the limitations in the accuracy of the data, one may nevertheless conclude that the best fit is obtained for  $\mathcal{I}/\mathcal{I}_{\text{rigid}} \approx 0.9$ .

The trend of the data points in Fig. 15 is approximately parallel to the curves of constant  $\mathcal{I}$ . A variation of  $\mathcal{I}$  with  $E$  would show up principally as a departure from this trend. To check the sensitivity of the analysis to such a variation, the possibility that  $\mathcal{I}/\mathcal{I}_{\text{rigid}}$  decreases with energy below the nucleon binding energy was considered. Some trial calculations were made using the expression

$$\mathcal{I}/\mathcal{I}_{\text{rigid}} = 1 - q \exp(-E/4), \quad (11)$$

with  $q$  taking on several values from 0 to 1.0, the maximum value that is physically reasonable. As may be seen from the dashed curves of Fig. 15, the results above about 6 MeV are very similar to those for  $q=0$  (i.e.,  $\mathcal{I}/\mathcal{I}_{\text{rigid}}=1.0$ ). The scatter of the data points below this

energy makes it difficult to draw conclusions. Better experimental data at low  $E$  would be needed to determine a value of  $q$  in this manner.

The results obtained from Figs. 13 and 15 and from similar analyses of the oxygen and sodium data are given in Table II. The estimates of error allow for the

TABLE II. Spin cutoff parameter  $\sigma$  and moment of inertia  $\mathcal{I}$  determined by comparison of experimental data with calculations of Ericson-Strutinski theory. The fourth column gives the range of residual-nucleus excitation energy  $E$  over which these fits were made.

Target	Bombarding energy (MeV)	Residual nucleus	Range of $E$ (MeV)	$\sigma$	$\mathcal{I}/\mathcal{I}_{\text{rigid}}$
$^{16}\text{O}$	27.2	$^{26}\text{Al}$	4 to 12	$2.6 \pm 0.6$	$0.7 \pm 0.4$
$^{16}\text{O}$	24.0	$^{26}\text{Al}$	4 to 12	$2.8 \pm 0.5$	$1.0 \pm 0.4$
$^{23}\text{Na}$	26.7	$^{32}\text{S}$	6 to 18	$3.0 \pm 0.6$	$0.9 \pm 0.3$
$^{27}\text{Al}$	26.6	$^{37}\text{Ar}$	6 to 20	$3.5 \pm 0.4$	$0.9 \pm 0.2$

uncertainties in the data. The results for the two sets of data for  $^{16}\text{O}$  are consistent within the errors. The selection of these best-fit values was made without regard to the absolute cross sections since only the ratios  $c_{2k}/c_0$  were considered. In effect this procedure discards an important piece of data, and in another paper<sup>24</sup> fits to absolute values as well as to shapes are demanded.

### C. Energy Dependence of Level Density

The usual method of determining the energy dependence of the level density is based on the relation given in (9). One obtains  $\rho(E,0)$  by dividing each datum point in the spectrum by  $\epsilon$  and  $\sigma_\epsilon(\epsilon)$ , thereby removing

<sup>31</sup> N. MacDonald, Atomic Weapons Research Establishment Report NR/P-2/61 (unpublished).

from the spectrum the uninteresting influences of phase space and transmission of the exit barrier. As we have seen, however, this simple relation is inaccurate if angular momentum is limited since then the decay of the compound nucleus is intimately connected with its mode of formation. No convenient method could be devised to analyze the spectra in a way which preserves the form of (5) and (6). Nevertheless we decided purely on a heuristic basis to apply (9) to the data because it does have the virtue of eliminating the factors which are uninteresting in this type of investigation. The analysis thus gives *apparent* level densities only. These apparent densities change with angle, as will be shown later.

The energy dependence of the level density has been treated theoretically by a number of authors, and formulas of varying degrees of sophistication are available.<sup>11</sup> In view of the difficulties just alluded to, we felt that fitting of the data to one of the more detailed forms of the level density would be unprofitable. Instead two extremely simple forms were used, namely

$$\rho_1(E,0) \sim \exp\{2[a_1(E-B_1)]^{1/2}\} \quad (12)$$

and

$$\rho_2(E,0) \sim \exp\{2[a_2(E-B_2)]^{1/2}\} / (E-B_2)^2. \quad (13)$$

The second of these is sometimes thought to be superior

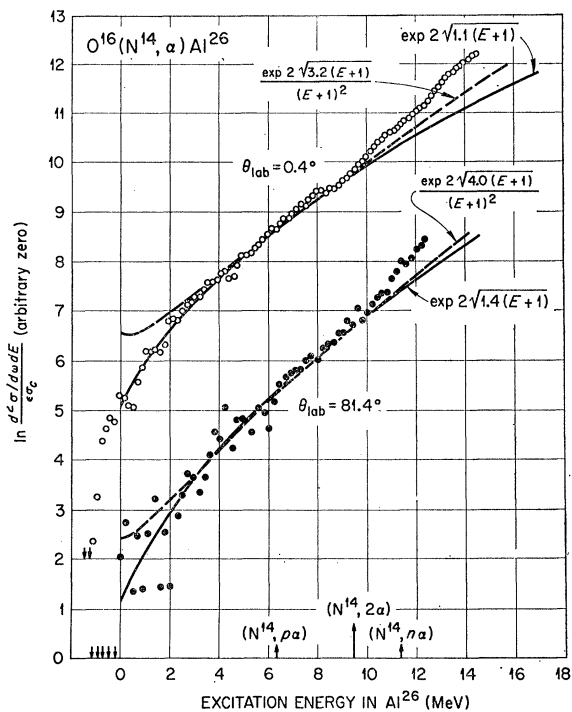


FIG. 16. Energy distributions at two angles of alpha particles from oxygen. Fits to two forms of the Fermi-gas level density are shown. The thresholds for alpha particles from secondary reactions are indicated by arrows pointing upward. The arrows pointing downward designate channels with zero counts in the original spectra.

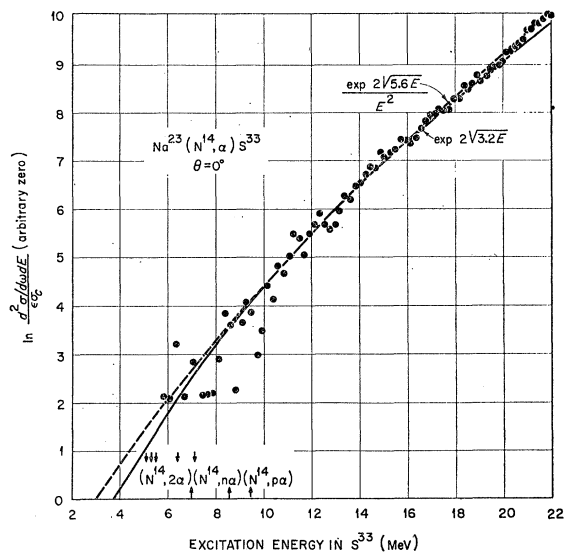


FIG. 17. Energy distributions at 0° of alpha particles from sodium. Fits to two forms of the Fermi-gas level density are shown. The thresholds for alpha particles from secondary reactions are indicated by arrows pointing upward. The arrows pointing downward designate channels with zero counts in the original spectra.

on theoretical grounds, but it should be used with care.<sup>32</sup> It is a high-energy approximation to a more accurate formula, and it is clearly quite unphysical near  $E=B_2$ . In the same spirit of approximate analysis, the values of  $\sigma_c(\epsilon)$  were taken from Blatt and Weisskopf<sup>33</sup> for a totally absorbing sphere with radius parameter  $1.5 \times 10^{-13}$  cm. The particle energies in the region of interest were always high enough for the asymptotic formula<sup>33</sup> to be used to calculate  $\sigma_c(\epsilon)$ .

Figure 16 shows the apparent level density obtained from  $^{16}\text{O}(^{14}\text{N},\alpha)$  at 0.4° lab (0.6° c.m.) and 81.4° lab (~100° c.m.). Except for the unphysical region of  $\rho_2$ , each is fit by both  $\rho_1$  and  $\rho_2$  with the parameters indicated. From the fits alone, there is little reason to prefer one to the other. The same comment may be made even more strongly for the other reactions studied, as seen in the examples of Figs. 17 and 18. A fit with a constant-temperature level density (a straight line on this plot) seems to be ruled out.

Each graph indicates the threshold energies for alpha particles from other reactions with the same target. The departure of the data from the theoretical curves at high excitation energy, which is especially noticeable in Fig. 16, is attributed to these secondary particles. Some of the data just above the lowest threshold for second-chance emission were used in making the fits shown in Figs. 16-18 because the exit Coulomb barrier effectively raises that threshold several MeV. Also, the intensity of second-chance emission just above this effective threshold should be quite small in comparison

<sup>32</sup> T. D. Thomas, Nucl. Phys. 53, 558 (1964).

<sup>33</sup> See Ref. 30, p. 352.

with that of the primary emission. The fits in Figs. 17 and 18 are good to remarkably high excitation energy, but the data above about 10 MeV were given no weight in making these fits.

The influence of second-chance emission on the angular distributions should also be considered. If second-chance emission is to be energetically possible, the first particle cannot be emitted with high energy and it cannot carry off much angular momentum. Consequently, the spin of the nucleus remains quite large and the anisotropy of the secondary particles will not be any weaker than that of the primaries.

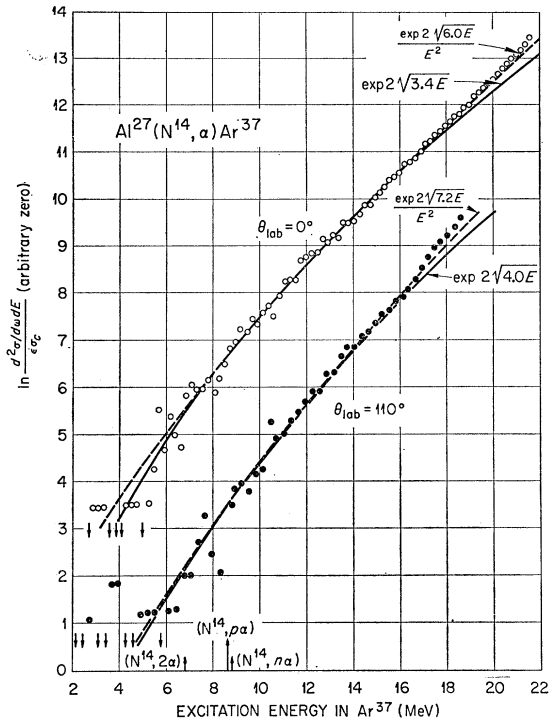


FIG. 18. Energy distributions at two angles of alpha particles from aluminum. Fits to two forms of the Fermi-gas level density are shown. The thresholds for alpha particles from secondary reactions are indicated by arrows pointing upward. The arrows pointing downward designate channels with zero counts in the original spectra.

Figures 16 and 18 show that the values of  $a_1$  and  $a_2$  do vary with angle, as anticipated. A more complete summary of the results may be seen in Figs. 19, 20, and 21. The abscissa is the center-of-mass angle averaged over each spectrum, to take account of the slight variation of c.m. angle with particle energy. The solid curves are symmetric about  $90^\circ$ , but otherwise have no theoretical significance.

The variation of the apparent level density is, however, not severe. The complete range of values of  $a_1$  and  $a_2$  is encompassed by a spread of about  $\pm 15\%$  from the mean value. We therefore expect that the mean value provides a reasonable estimate of the energy

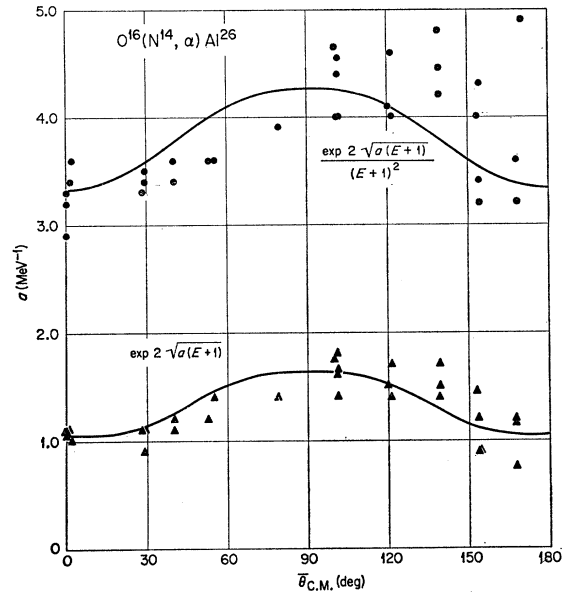


FIG. 19. Best-fit values of the level-density parameters for alphas from oxygen as a function of average center-of-mass angle.

variation of the true level density. The calculated angular distributions were quite insensitive to  $a$ ; doubling  $a$  for the alpha-particle channel in the reaction with

TABLE III. Angle-averaged parameters for the two forms of the Fermi-gas level density defined in (12) and (13). The symbol  $A$  is the mass number of the residual nucleus.

Target	Residual nucleus	$B_1$ (MeV)	$a_1$ (MeV <sup>-1</sup> )	$A/a_1$ (MeV)	$B_2$ (MeV)	$a_2$ (MeV <sup>-1</sup> )	$A/a_2$ (MeV)
<sup>16</sup> O	<sup>26</sup> Al	-1	1.3	20.0	-1	3.8	6.8
<sup>28</sup> Na	<sup>38</sup> S	0	3.5	9.4	0	5.5	6.0
<sup>27</sup> Al	<sup>37</sup> Ar	0	3.6	10.3	0	6.0	6.2

oxygen was equivalent to only a 15% change in  $\mathcal{G}/\mathcal{G}_{\text{rigid}}$ . Table III lists the values of  $a_1$  and  $a_2$  averaged over

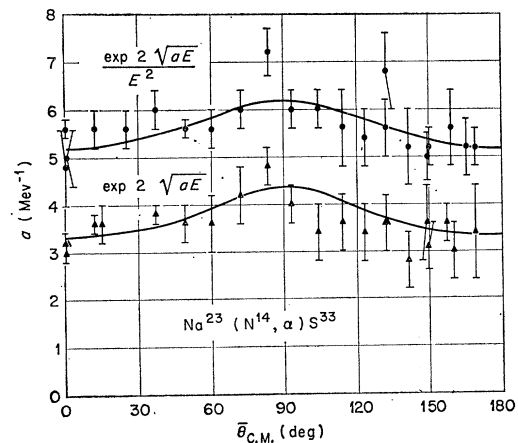


FIG. 20. Best-fit values of the level-density parameters for alphas from sodium as a function of average center-of-mass angle.

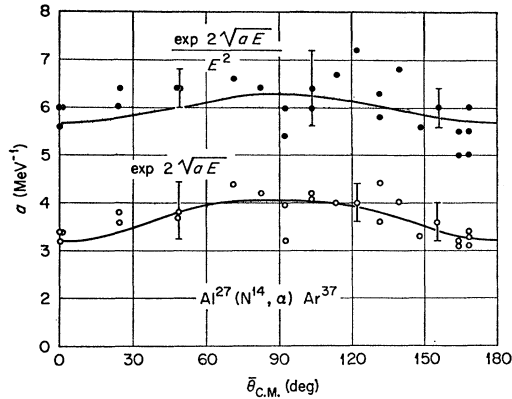


FIG. 21. Best-fit values of the level-density parameters for alphas from aluminum as a function of average center-of-mass angle.

angles. Since these parameters should be proportional to mass number  $A$  (neglecting shell effects), the results divided by  $A$  are also listed. The values of  $A/a_1$  for  $^{33}\text{S}$  and  $^{37}\text{Ar}$  are in good agreement with the empirical relation<sup>34</sup>  $a_1 \approx A/10$ .

#### V. SUMMARY

The  $(^{14}\text{N}, \alpha)$  reactions on  $^{16}\text{O}$ ,  $^{23}\text{Na}$ , and  $^{27}\text{Al}$  targets are characteristic of compound-nucleus processes in the continuum region. The angular distributions are symmetric about  $90^\circ$ , while the energy spectra are smooth and show very few transitions directly to low-lying states. Pronounced forward-backward peaking is seen, due to the high angular momentum involved.

A semiclassical statistical-model analysis of the angular distributions shows that the spin cutoff parameter  $\sigma$  in the level density of the corresponding residual nuclei  $^{26}\text{Al}$ ,  $^{33}\text{S}$ , and  $^{37}\text{Ar}$  varies from about 2.6 to 3.5. The moment of inertia is close to the rigid-body value. This indicates that rotation of the nucleus involves all the nucleons rather than just a portion of them, since it has been shown that a gas of rotating fermions will have the rigid-body moment of inertia if their relative motion is random.<sup>35</sup> This provides further support for the use of the compound-nucleus picture for these reactions.

The energy spectra of the alpha particles emitted from the sodium and aluminum targets are consistent with statistical decay to residual nuclei having a level density varying approximately as  $\exp[2(a_1 E)^{1/2}]$ , with  $a_1 \approx A/10$ . Equally good fits are obtained with  $a_2 \approx A/6$  in the expression  $(E)^{-2} \exp[2(a_2 E)^{1/2}]$ .

#### ACKNOWLEDGMENTS

We wish to thank A. Zucker for advice and continuing interest at all stages of this research, R. H. Bassel and

<sup>34</sup> J. M. B. Lang and K. LeCouteur, Proc. Phys. Soc. (London) **A67**, 586 (1954).

<sup>35</sup> R. M. Rockmore, Phys. Rev. **116**, 469 (1959). See also M. A. Preston, *Physics of the Nucleus* (Addison-Wesley Publishing Company, Inc., Reading, Massachusetts, 1962), p. 280.

R. M. Drisko for the optical-model programs and instruction in their use, H. F. Bowsher for supervising the calculation of the transmission coefficients and for comments on the manuscript, B. D. Williams and F. L. Miller for writing the data-processing programs, J. L. Blankenship for furnishing the silicon detector, G. A. Palmer for assistance in taking data and performing calculations, and the crew of the ORNL 63-in. Cyclotron for their efforts in providing a good beam. Discussions of theoretical points with A. C. Douglas, T. Ericson, E. C. Halbert, D. W. Lang, and N. MacDonald were helpful at various times during this research.

#### APPENDIX 1

Evaluation of (5) is extremely laborious when many angular momenta are involved. Accordingly, a FORTRAN program was written to perform the calculations on an IBM 7090. Four exit channels were considered, those involving emission of neutrons, protons, deuterons, and alpha particles. Although the program allows flexibility in the choice of parameters, in most cases the same value of  $\sigma$  (or  $g/g_{\text{rigid}}$ ) was used for all exit channels. Running time for computing  $c_0, c_2, \dots, c_8$  at 11 values of  $E$  is about 1.6 min for each choice of  $\sigma$ .

Certain parameters in addition to  $\sigma$  (or  $g$ ) must be specified in order to evaluate (5) and (6). The transmission coefficients were obtained from optical-model programs. In a few cases elastic scattering measurements were available and the optical parameters could be chosen on a firm basis. Figure 1 is an example of the transmission coefficients for one of these well-established cases,  $^{14}\text{N}$  on  $^{27}\text{Al}$ . The optical model used here was selected by a multiparameter search<sup>36</sup> for a best fit to the experimental data.<sup>37</sup> However, most of the exit channels involved unstable nuclei, in excited states, and covered a wide range of channel energy. For these systems, interpolation and/or extrapolation from optical parameters of known systems were necessary.

Table IV lists the optical-model parameters used to generate the  $T_l$  for the Ericson-Strutinski calculation. The definitions of the symbols are as follows. The optical potential was the sum of three terms: a real nuclear potential, an imaginary potential, and a Coulomb potential. The first of these was always of Saxon-Woods form

$$V\{1 + \exp[(r - r_0 A_t^{1/3})/a]\}^{-1},$$

where  $A_t$  is the mass number of the target. For the proton and neutron channels, the parameter  $V$  was dependent on the channel energy  $\epsilon$ . The shape of the imaginary well was either of the Saxon-Woods type or was the derivative of a Saxon-Woods well

$$[W + W'd/dx'](e^{x'} + 1)^{-1},$$

where

$$x' = (r - r_0' A_t^{1/3})/a'.$$

<sup>36</sup> R. H. Bassel (private communication).

<sup>37</sup> M. L. Halbert and A. Zucker, Nucl. Phys. **16**, 158 (1960).

TABLE IV. Optical-model parameters.

Channel	$V$ (MeV)	$r_0$ (fermi)	$a$ (fermi)	$W$ (MeV)	$W'$ (MeV)	$r_0'$ (fermi)	$a'$ (fermi)	$r_c$ (fermi)
$^{14}\text{N}+^{16}\text{O}$	48	2.49	0.575	5.75	0	2.49	0.575	1.64
$p+^{29}\text{Si}$	$57.4-0.3\epsilon$	1.047	0.675	0	22.2	1.468	0.611	1.25
$n+^{29}\text{P}$	$52.6-0.3\epsilon$	1.047	0.675	0	22.2	1.468	0.611	...
$d+^{28}\text{Si}$	73.6	1.157	0.764	0	81.51	1.397	0.658	1.157
$\alpha+^{26}\text{Al}$	49.0	1.80	0.530	6.5	0	1.80	0.530	1.80
$^{14}\text{N}+^{23}\text{Na}$	47.5	1.89	0.661	3.39	0	1.89	0.661	1.20
$p+^{36}\text{Cl}$	$57.3-0.3\epsilon$	1.047	0.675	0	22.2	1.468	0.611	1.25
$n+^{36}\text{Ar}$	$51.8-0.3\epsilon$	1.047	0.675	0	22.2	1.468	0.611	...
$d+^{35}\text{Cl}$	58.0	1.06	1.012	0	51.26	1.502	0.599	1.06
$\alpha+^{33}\text{S}$	45.0	1.70	0.52	10.0	0	1.70	0.52	1.7
$^{14}\text{N}+^{27}\text{Al}$	39.6	2.12	0.626	27.5	0	2.12	0.626	1.0
$p+^{40}\text{K}$	$57.3-0.3\epsilon$	1.047	0.675	0	22.2	1.468	0.611	1.25
$n+^{40}\text{Ca}$	$51.4-0.3\epsilon$	1.047	0.675	0	22.2	1.468	0.611	...
$d+^{39}\text{K}$	58.0	1.06	1.012	0	51.26	1.502	0.599	1.06
$\alpha+^{37}\text{Ar}$	45.0	1.7	0.52	10.0	0	1.7	0.52	1.7

The Coulomb potential was that of a point charge incident on a uniformly charged sphere of radius  $r_c A^{1/3}$ .

In the ratio  $F/\sum F$  of (5), the competition of various exit channels as a function of  $I$  is strongly influenced by the level-density parameters. Both the energy dependence of  $\rho(E,0)$  and the constant of proportionality omitted from (12) and (13) are significant here. The results of Table II were obtained with the form  $\rho_1(E,0)$  given by (12). The values of  $a_1$  and  $B_1$  for the alpha-particle channel were taken from the analysis of the energy spectra described in IV C. For the other exit channels, data from earlier experiments in some cases provided values for  $a_1$  and  $B_1$  directly<sup>20,21</sup>; for the rest, interpolation from previous data was necessary. As mentioned earlier, the angular distributions are insensitive to  $a_1$ . Table V lists the parameters actually used in most of the calculations.

The approximation  $\rho_1(E,0)$  used in these calculations,

TABLE V. Level-density parameters used in the Ericson-Strutinski calculations. The last column gives the relative constants of proportionality assigned to the level densities of the various exit channels.

Target	Exit channel	$a_1$ (MeV <sup>-1</sup> )	$B_1$ (MeV)	Relative proportionality constant
$^{16}\text{O}$	$\alpha+^{26}\text{Al}$	1.33	-1	1.0
	$p+^{29}\text{Si}$	2.5	0	1.0
	$n+^{29}\text{P}$	2.5	0	1.0
	$d+^{28}\text{Si}$	1.8	0	0.5
$^{23}\text{Na}$	$\alpha+^{33}\text{S}$	3.53	0	1.0
	$p+^{36}\text{Cl}$	4.0	0	2.0
	$n+^{36}\text{Ar}$	4.0	0	0.5
	$d+^{35}\text{Cl}$	3.89	0	1.0
$^{27}\text{Al}$	$\alpha+^{37}\text{Ar}$	3.56	0	1.0
	$p+^{40}\text{K}$	5.0	0	2.5
	$n+^{40}\text{Ca}$	5.0	0	0.5
	$d+^{39}\text{K}$	4.33	0	1.0

through crude from a theoretical point of view, nevertheless gives an excellent empirical summary of the energy spectra. Some of the calculations were repeated using a modification of  $\rho_2(E,0)$  which eliminated the unphysical upturn at low  $E$ ; the best-fit moments of inertia were within the uncertainties listed in Table II.

The constant of proportionality in  $\rho(E,0)$  must also be specified for all exit channels of a given compound nucleus. Actually, the only quantities needed here are the ratios of these constants. The values actually used are given in Table V. Previous data provided these numbers for the  $p$ ,  $d$ , and  $\alpha$  channels in the  $^{16}\text{O}$  reactions<sup>20</sup> and for the  $p$  and  $\alpha$  channels in the  $^{27}\text{Al}$  reactions.<sup>21</sup> Allowance was made for the 1-MeV shift of the effective zero of excitation for alpha particles from  $^{16}\text{O}$ , which reduces the proportionality factor needed to reproduce the observed<sup>20</sup> relative intensity of protons and alpha particles. The proportionality constants for the  $^{23}\text{Na}$  reactions are based on the assumption that odd- $A$  nuclei have a level density twice that of even-even nuclei, while odd-odd nuclei have about four times as many levels as even-even nuclei. The results seem to be insensitive to this parameter. Calculations for  $^{27}\text{Al}(^{14}\text{N},\alpha)^{37}\text{Ar}$  with 1:5:12 ratios instead of 0.5:1:2.5 give  $c_{2k}/c_0$  which are identical within a few percent.

## APPENDIX 2

For some purposes, approximations to the Ericson-Strutinski angular distribution  $W(\theta)$  may be useful. The original paper<sup>9</sup> gives an approximation suitable for weak anisotropy

$$W(\theta) \approx 1 + \langle I^2 \rangle \langle l^2 \rangle / 8\sigma^4 \cos^2\theta,$$

where  $\langle I^2 \rangle$  and  $\langle l^2 \rangle$  are averages weighted according to  $IT_I$  and  $lT_l$ .

If the significant contributions in the original expression<sup>9</sup> arise from small values of  $Il/\sigma^2$ , one can expand the Bessel function in a power series and integrate

term by term, with the result<sup>38</sup>

$$W(\theta) = [1 + \frac{2}{3}\beta^{(2)} + (2/15)\beta^{(4)} + \dots]P_0(\cos\theta) \\ + [\frac{1}{3}\beta^{(2)} + (2/21)\beta^{(4)} + \dots]P_2(\cos\theta) \\ + [(1/35)\beta^{(4)} + \dots]P_4(\cos\theta) \\ + \dots \quad (14)$$

In this expression

$$\beta^{(2k)} = \langle I^{2k} \rangle \langle l^{2k} \rangle / (2\sigma^2)^{2k},$$

where the averages over  $I^{2k}$  and  $l^{2k}$  are weighted by  $IT_I \exp(-I^2/2\sigma^2) / [\rho_c(I)\Gamma_I]$  and  $lT_l \exp(-l^2/2\sigma^2)$ ,

<sup>38</sup> E. C. Halbert (private communication).

respectively. In the first weighting factor,  $\rho_c(I)$  is the density, and  $\Gamma_I$  the decay width, of compound states with spin  $I$ .

A similar expansion with terms up to  $P_6(\cos\theta)$  has been published elsewhere.<sup>6</sup> However, two questionable approximations were made in obtaining the result. First, each of the  $\beta^{(2k)}$  was replaced by  $[\beta^{(2)}]^k$ . Second, the published formula includes only the first term of each square bracket in (14), thereby omitting terms of the same order as those it retains. If  $\beta^{(2)} \gtrsim 1$ , the coefficients of  $P_4$  and  $P_6$  are small, but clearly one cannot now omit the term  $(\frac{2}{3})\beta^{(2)}$  in the coefficient of  $P_0$ . The  $\beta^{(4)}$  terms in the  $P_0$  and  $P_2$  coefficients may also be significant. It should be noted that  $\beta^{(2)}$  is likely to be of order unity whenever the anisotropy is easily visible.

## Electron Scattering by Calcium at 250 MeV\*

M. CROISSIAUX,† R. HOFSTADTER, A. E. WALKER, AND M. R. YEARIAN  
*Stanford University, Stanford, California*

AND

D. G. RAVENHALL‡  
*Università di Roma, Roma, Italy and University of Illinois, Urbana, Illinois*

AND

B. C. CLARK AND R. HERMAN  
*General Motors Corporation, Warren, Michigan*  
(Received 25 September 1964)

The doubly magic nucleus of  $\text{Ca}^{40}$  has been investigated by the electron scattering technique at an incident energy of 250 MeV. The elastic scattering behavior has been resolved from the inelastic scattering, and absolute data on cross sections have been obtained for both types of events. In the case of the elastic scattering, the first and second diffraction features have been observed and measured. It has been possible to make a comparison of the elastic data with theoretical calculations based on a phase-shift analysis for certain assumed models of the nuclear charge density distribution. The combination of such an analysis with the present data, and also with earlier data on the same nucleus, permits the determination of the radius and skin thickness of the  $\text{Ca}^{40}$  nucleus with a precision greater than has been attainable heretofore. An investigation of the dependence of the density distribution on a third parameter indicates that a Fermi distribution, or models close to this type, are required to fit the experimental data. A Fermi radial charge density distribution with radius  $c = 3.60$  F and skin thickness  $t = 2.50$  F fits the data extremely well.

### I. INTRODUCTION

IT has been clear for some time that the behavior of the charge density in the ground states of many spherically symmetric nuclei of the periodic system can be reasonably well described by a distribution function approximately constant from the center of the nucleus ( $r=0$ ) to the neighborhood of the surface region where

the density gradually drops to the value zero. The distribution is characterized by the two parameters  $c$  and  $t$ , which represent, respectively, the distance to the half-density point and the 90%–10% “skin thickness.”<sup>1</sup> The evaluation of  $c$  and  $t$  is effectively related to the description of the charge density in the vicinity of the surface, and it is therefore the surface behavior that is best determined by the analyses of the previous published data. It is clearly desirable to know more about the behavior of the density function near the

\* This work was supported in part by the Office of Naval Research, and the U. S. National Science Foundation.

† Now at Centre de Recherches Nucléaires, Strasbourg-Cronenburg, France.

‡ On sabbatical leave from the University of Illinois, Urbana, Illinois during 1963–64.

<sup>1</sup> B. Hahn, D. G. Ravenhall, and R. Hofstadter, *Phys. Rev.* **101**, 1131 (1956).